JOURNAL OF CATALYSIS 112, 345–356 (1988)

A Dynamic Study of the Water–Gas Shift Reaction over an Industrial Ferrochrome Catalyst

T. SALMI, S. BOSTRÖM, AND L.-E. LINDFORS

Laboratory of Industrial Chemistry, Department of Chemical Engineering, Åbo Akademi, SF-20500 Turku, Finland

Received August 28, 1987; revised February 15, 1988

The water–gas shift reaction over an industrial ferrochrome catalyst (ICI 15-4) was studied by transient experiments in a gradientless spinning basket reactor at 563–638 K and atmospheric pressure. The responses of CO, CO_2, and H_2 were measured after step changes at the reactor inlet. The stationary kinetics were described with a first-order rate expression with respect to CO. The rate constants were determined at four temperatures. The CO_2 responses followed approximately a first-order behavior, whereas the dynamics of the H_2 liberation was always slower than the CO_2 evolution. Hydrogen formation was retarded by H_2O pretreatment of the catalyst. Two characteristic values of the total oxygen transfer through the catalyst were determined from the CO_2 and H_2 responses, corresponding to the catalyst pretreatments with the reactive gases (CO and H_2O) and with H_2O. The transient responses were modeled with a reaction mechanism involving rapid water adsorption and slow CO interconversion and H_2 desorption steps. The kinetic parameters of the simplified dynamic model were determined by regression analysis. The shift reactor start-up and shut-down could be predicted by the dynamic model developed.

INTRODUCTION

Chromia-promoted magnetite is frequently used to catalyze the water–gas shift reaction

$$CO + H_2O \rightleftarrows CO_2 + H_2 \qquad (1)$$

in industrial processes (*1*). Several publications (*2–9*) concern the stationary kinetics of the reaction. These kinds of investigations, in spite of their usefulness in reactor analysis and design, cannot give very much information about the elementary reaction steps proceeding on the catalyst surface. Insight into the reaction mechanism can be obtained by isotopic exchange experiments under equilibrium conditions or by transient experiments studying the reactor start-up and shut-down after different catalyst pretreatments.

Boreskov and co-workers (*10*) studied reaction (1) dynamically by measuring separately the catalyst oxidation and reduction rates. Oki and co-workers (*11–13*) used isotope labeling to elucidate the reaction mechanism. Recently the dynamic studies have been continued by Tinkle and Dumesic (*15*) and by the present authors (*16*). We reported (*16*) preliminary results from reactor start-up studies after different catalyst pretreatment procedures and Tinkle and Dumesic (*15*) published the results of isotopic exchange experiments and proposed a model for the reaction mechanism. The key point in the discussion concerning the reaction mechanism is whether the reaction proceeds through a regenerative (oxidative–reductive) (*5, 10, 15, 16*) or an adsorptive (*11–13, 15–16*) pathway. In the present work the results of the transient experiments are analyzed by systematic modeling to obtain a discrimination between different reaction mechanisms, to estimate rate parameters, and to obtain guidelines for prediction of the dynamics of shift reactors.

EXPERIMENTAL

A commerical ferrochrome catalyst (ICI 15-4) was used in all the experiments. The pellets were crushed and sieved to particles

0021-9517/88 $3.00

with diameters between 0.6 and 1.0 mm. Reagent-grade gas containing 8.05% CO in N_2 obtained from AGA Ab was used as received. Distilled and ion-exchanged water was fed to the reactor with an HPLC pump.

The reactor was a gradientless spinning basket reactor from Autoclave Engineers Inc. with an empty volume of 345 ml. The mass of the fresh catalyst was 32.2 g. The gases were fed through a preheater to the reactor. A condenser working at 273 K was placed at the reactor outlet for separation of unreacted water. The outlet gas was analyzed with a gas chromatograph equipped with a TC detector and a packed Chromosorb 102 column. Nitrogen was used as carrier gas instead of He to obtain good sensitivity for H_2. CO_2 and H_2 were analyzed chromatographically, whereas the CO content of the product gas was determined by an IR analyzer. An automatic microcomputer-based data acquisition system was developed for collection and processing the large body of transient data. The experimental equipment is described in detail in our previous paper (*16*).

The kinetic experiments were performed at four temperatures (563, 592, 624 and 638 K) in random order at atmospheric pressure. The molar ratio between inlet H_2O and CO was varied approximately from 2 to 12. The reactor space time was typically about 1.6 min. The transient experiment was continued until the reactor steady state was achieved with certainty (about 1 h) in order to measure also the stationary reaction rate. The transient experiment was started either by switching the N_2 flow to a $CO/N_2/H_2O$ flow or, after a water pretreatment, by switching the N_2/H_2O flow to a $CO/N_2/H_2O$ flow. Typical transient experiments are illustrated in Fig. 2.

RESULTS AND DISCUSSION

Physical investigations of the fresh and the used catalysts, namely low-temperature nitrogen adsorption and SEM studies, showed that no sintering or other loss of surface area occurred during the kinetic experiments. ESCA analysis verified the coexistence of di- and trivalent iron on the catalyst surface. The physically determined catalyst properties are given in Table 1.

TABLE 1

Catalyst (ICI 15-4) Properties and Reactor Parameters

Catalyst density (ρ_c)	3.98 g cm^{-3}
Catalyst surface area (σ)	108 m^2 g^{-1}
Catalyst monolayer capacity	0.82 cm^3 N_2 (1 atm, 273 K)
Catalyst mass in reactor	33.2 g
Reactor volume	345 cm^3
Reactor space time (τ)	1.4–1.8 min
Void fraction (ε)	0.98

The stationary and step response experiments are used for quantitative modeling of the shift reaction. The material balance around a gradientless spinning basket reactor can be written as

$$d\mathbf{x}/d\Theta = -(\mathbf{x} - \mathbf{x}_0)/\varepsilon + A\mathbf{r} \qquad (2)$$

$$d\mathbf{c}*/d\Theta = \tau\mathbf{r}* \qquad (3)$$

where $\mathbf{x}$ and $\mathbf{c}*$ denote the mole fractions of the gas-phase components and the concentrations of adsorbed surface intermediates, respectively. Other quantities are as defined under Nomenclature. At steady state the time derivatives in Eqs. (2) and (3) disappear. The stationary reaction rate can thus be calculated from

$$\mathbf{r}(\mathbf{x}, \mathbf{k}, \mathbf{K}) = (\mathbf{x} - \mathbf{x}_0)/(A\varepsilon), \qquad (4)$$

where $\mathbf{k}$ and $\mathbf{K}$ denote the rate and equilibrium constants of the elementary steps.

Stationary Kinetics

The steady-state reaction rate was observed to be proportional to the carbon monoxide concentration, whereas it was practically independent of the water concentration. A suitable trial function for description of the steady-state behavior is therefore the simple first-order rate law

$$r_{CO} = k_{CO}x_{CO}P(1 - \beta), \qquad (5)$$

where P is the total pressure and β is a factor to account for the effect of the reversible reaction; $\beta = x_{CO_2}x_{H_2}/(Kx_{CO}x_{H_2O})$.

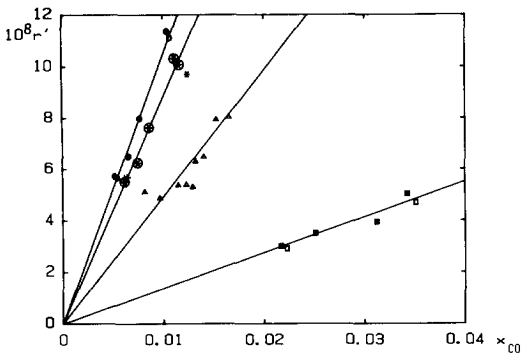

FIG. 1. The dependence of steady-state reaction rate ($r' = r/(1 - \beta)$, Eq. (5)) on the partial pressure of CO at 563 K (□, ■), 592 K (△, ▲), 624 K (*, ⊛), and 638 K (○, ●). Open symbols (□, △, *, ○) denote water pretreatment.

The temperature dependence of the equilibrium constant (K) is given by Moe (*4*). The test plots of the rate data obtained at four temperatures are shown in Fig. 1. The validity of the rate expression (5) at the actual concentration range is obvious. The pretreatment of the catalyst with water did not affect the stationary reaction rate, as can be seen from Fig. 1. The rate constants computed from Eq. (5) with regression are listed in Table 2.

There appears, however, to be a discrepancy in attempting to fit the constants to the Arrhenius law: the Arrhenius plot is bent when approaching the highest temperatures (624 and 638 K). Two principal explanations are possible: either the constant k_{CO} is not a fundamental kinetic constant but a lumped parameter or the reaction rate is influenced by diffusional resistances at the higher temperatures. An estimation of the activation energy from rate constants obtained at 563 and 592 K gives E_a = 122 kJ/mol which is in accordance with the values given by several previous authors (*7, 9, 17–20*). On the other hand, much lower values for the activation energy have been reported (*4, 21*). Those results were, however, obtained from experiments performed at temperatures up to 670 K. Our results probably incorporate the contradictory observations of the previous investigators. In order to give a further explanation of the observed stationary kinetics it is necessary to analyze the transient behavior of the system.

TABLE 2

First-Order Rate Constants according to Eq. (5)

T (K)	$10^6\, k_{CO}$ (mol m^{-2} min^{-1} atm^{-1})
563	1.38
592	4.92
624	8.79
638	10.40

General Characteristics of Step Responses

Three basic types of step response were observed. The response types are shown in Fig. 2, where the mole fraction x is plotted against Θ, the dimensionless time t/τ. A common feature in all responses is the slower liberation of H_2 than that of the CO_2 formation. If the catalyst was pretreated for

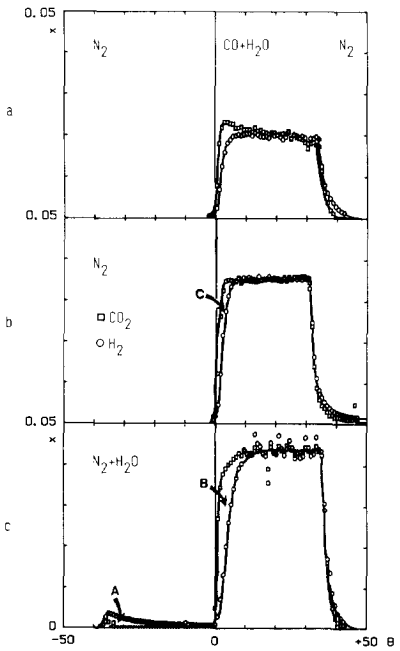

FIG. 2. The principal types of transient experiment.

a short time (15 min) with the reaction mixture (CO, H_2O, N_2) (Fig. 2b) or for a longer time (1–2 h) with water (Fig. 2c) a monotonically increasing response of CO_2 was observed. If the experiment was started directly after a N_2 exposure a slight overshoot appeared in the CO_2 response (Fig. 2a). This type of response was not very easy to reproduce; it was probably due to the partial reduction of the catalyst during the transient, i.e., the formation of CO_2 from CO and lattice oxygen. The responses in Figs. 2b and 2c have the same form; the retardation of hydrogen evolution is, however, much more apparent after the water exposure (Fig. 2c). During the water preadsorption period small amounts of hydrogen ($x_{H_2,max} = 0.003$) were always liberated, as can be seen in Fig. 2c. The number of surface sites covered by oxygen obviously increased during the water pretreatment, whereas the number of sites for water adsorption and cleavage decreased. These effects caused the retardation of the hydrogen evolution when the shift reaction was started. At the reactor shut-down the decay of the CO_2 response was always faster than the decay of the H_2 response.

Oxygen Transfer through the Catalyst

The difference between CO_2 and H_2 responses is used for estimation of the oxygen transfer through the catalyst. This evaluation can be made without assuming any particular reaction mechanism for the shift process. The net rate of oxygen transfer is equal to the difference of the formation rates of H_2 and CO_2:

$$r^*_O = r_{H_2} - r_{CO_2}. \quad (6)$$

Equation (6) is inserted in the material balance (3) giving

$$dc^*_O/d\Theta = \tau(r_{H_2} - r_{CO_2}) \quad (7)$$

which is integrated from $\Theta = 0$ to $\Theta = \infty$ (steady state) to obtain the total oxygen change, Δc^*_O. The rate difference $r_{H_2} - r_{CO_2}$ can be computed from the material balances:

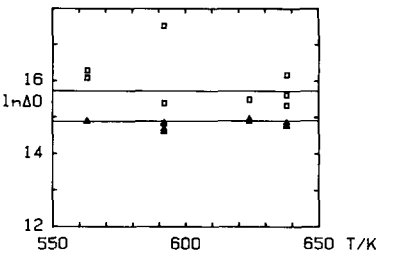

FIG. 3. The total surface oxygen change ($\Delta 0$) determined from experiments with ($\triangle$) and without water pretreatment ($\square$).

$$r_{H_2} - r_{CO_2} = (dx_{H_2}/d\Theta - dx_{CO_2}/d\Theta + (x_{H_2} - x_{CO_2})/\varepsilon)/A. \quad (8)$$

The integral of Eq. (8) is represented by

$$\int_0^\infty (r_{H_2} - r_{CO_2})d\Theta = \int_0^\infty (x_{H_2} - x_{CO_2})/(A\varepsilon)d\Theta \quad (9)$$

because $\int_0^x dx_{H_2} - \int_0^x dx_{CO_2} = 0$; x denotes here the steady-state mole fractions of H_2 and CO_2, which were equal in every experiment. The operative form for computation of the oxygen change can thus be written as

$$-\Delta c^*_O = P/(\sigma\rho_c(1 - \varepsilon)RT) \int_0^\infty (x_{CO_2} - x_{H_2})d\Theta. \quad (10)$$

The numerical integration of the experimental responses gave the results plotted in Fig. 3. Two typical levels of Δc^*_O are observed, approximately 3.7×10^{-7} and 0.98×10^{-7} mol/m^2 corresponding to the experiments with and without water preadsorption. These surface oxygen changes represent 3.3 and 0.88% of the monolayer capacity determined by nitrogen adsorption at 77 K. The surface oxygen change seems to be independent of the concentrations of CO and H_2O at the actual experimental region. The oxygen change is also practically independent of the temperature as can be seen from Fig. 3.

Hydrogen was liberated during the water preadsorption period, which implies an increase in the oxygen content of the cata-

lyst. If the hydrogen response during the preadsorption is integrated (area A in Fig. 2c) and this area is subtracted from the integrated difference between the CO_2 and H_2 responses (area B in Fig. 2c) the result should be the integrated difference between CO_2 and H_2 obtained from the corresponding experiment without water pretreatment (area C in Fig. 2b). Calculations showed that this hypothesis could be confirmed at least qualitatively; difficulties arose in integration of the H_2 response during the preadsorption period since the detection limit of H_2 was approached. The results indicate, however, that the catalyst had approximately the same initial state before the experiments, i.e., before starting the shift reaction (Fig. 2b) or water adsorption (Fig. 2c).

Reaction Mechanisms

The first-order steady-state kinetics, the principally identical forms of step responses within the experimental domain, and the independence of the total surface oxygen transfer of the steady-state gas-phase composition indicate that the same reaction mechanism is valid in the investigated range of temperatures and concentrations. Two different pathways have been proposed for the high-temperature water–gas shift reaction: a regenerative (*5*, *10*) and an adsorptive (*11–13*) pathway. These mechanisms are thoroughly discussed in our previous publication (*16*). Recently Tinkle and Dumesic (*15*) suggested a mechanism combining adsorptive and regenerative reaction steps. The adsorptive mechanism of Oki and co-workers (*11–13*) was criticized by us (*16*) because it would predict an increase in the hydrogen liberation rate after water preadsorption, whereas we observed a decrease in H_2 evolution rate after water exposure. On the other hand, Oki *et al.* suggested (*11–13*) that hydrogen desorption might be a slow reaction step which is consistent also with our data. The regenerative mechanism of Shchibrya and co-workers (*5*)

$$\begin{aligned} CO + O* &\rightleftarrows CO_2 + * \\ H_2O + * &\rightleftarrows H_2 + O* \end{aligned} \qquad (11)$$

would predict the retardation of the H_2 response after a H_2O exposure, because vacant sites (*) are oxidized by water. It has, however, later been proved (*22*) that reactive components (CO, CO_2, H_2O) adsorb on the catalyst under the reaction conditions. The independence of the reaction rate of the water pressure also suggests a rapid adsorption step for H_2O, whereas the water cleavage and hydrogen desorption steps are rate determining in hydrogen evolution. We therefore proposed (*16*) the following mechanism for the shift process:

$$CO + O*_2 \rightleftarrows CO_2(*)_2 \qquad \text{(I)}$$

$$CO_2(*)_2 \rightleftarrows CO_2 + (*)_2 \qquad \text{(II)}$$

$$H_2O + (*)_1 \rightleftarrows H_2O(*)_1 \qquad \text{(III)}$$

$$H_2O(*)_1 + (*)_1 + (*)_2 \rightleftarrows 2H(*)_1 + O(*)_2 \qquad \text{(IV)}$$

$$2H(*)_1 \rightleftarrows H_2 + 2(*)_1 \qquad \text{(V)} \qquad (12)$$

where $(*)_1$ and $(*)_2$ denote different sites for CO and H_2O adsorption. The adsorption step (III) is assumed to be rapid, whereas the other steps are slow, thereby controlling the formation of CO_2 and H_2. The mechanism suggested recently by Tinkle and Dumesic (*15*) can be written as

$$\begin{aligned} CO + (*)_2 &\rightleftarrows CO_2(*)_2 && \text{(I)} \\ CO_2(*)_2 &\rightleftarrows CO_2 + (*)_1 && \text{(II)} \\ H_2O + (*)_1 &\rightleftarrows H_2O(*)_1 && \text{(III)} \\ H_2O(*)_1 + (*)_2 &\rightleftarrows 2H(*)_2 && \text{(IV)} \\ 2H(*)_2 &\rightleftarrows H_2 + 2(*)_2 && \text{(V)} \end{aligned} \qquad (13)$$

The water adsorption (III) and cleavage (IV) steps were assumed to be fast. The sites denoted by $(*)_2$ contain a surface oxygen. The similarities of mechanisms (12) and (13) are obvious: both models predict a reactive adsorption of CO and CO_2 with an indistinguishable surface intermediate

$[CO_2(*)_2]$, a fast adsorption of H_2O, and a slow associative desorption of hydrogen. The difference between (12) and (13) appears only in the interconversion step of water (step IV in Eqs. (12) and (13)). Tinkle and Dumesic (*15*) give a reasonable explanation for the chemical character of the sites $(*)_1$ and $(*)_2$ in (13): $(*)_2$ represents a metal oxide site with surface oxygen, whereas $(*)_1$ denotes the same site without oxygen, and $CO_2(*)_2$ is a bidentate carbonate. The essential feature in both mechanisms (12) and (13) is the blocking of vacant sites by adsorbed H_2O and hydrogen. On the other hand, the validity of the first-order stationary reaction rate expression (5) suggests that the conversion of CO is the slowest reaction step and that the change of the surface oxygen capacity during the reaction is minor.

Modeling of CO_2 and H_2 Responses

Mechanisms (12) and (13) involving five elementary steps contain too many parameters to be determined simultaneously. We shall therefore proceed toward the simplest possible model for description of the observed transient responses. Since the sum of the CO and CO_2 responses behaved almost like an inert tracer during the transients, as shown in the previous paper (*16*), the adsorption of CO and CO_2 is assumed to be negligible compared to the adsorption of water. It is further assumed that the surface oxygen content is large compared to the number of vacant sites and that the reversible reaction is negligible [$(1 - \beta)$ in Eq. (5) is close to 1]. The steps for CO_2 formation are thus simplified to

$$CO + O* \rightarrow CO_2 + * \qquad (14)$$

The reaction rate of CO_2 is

$$r_{CO_2} = -r_{CO} = kx_{CO}Pc*_O, \qquad (15)$$

where $kc*_O$ is approximated by k_1, a first-order rate constant. After (15) is inserted in the material balances of CO and CO_2 the simple models (16) and (17) for CO and CO_2 responses are obtained:

$$x_{CO} = x_0\tau_1(1 - \exp(-\Theta/\tau_1)/\varepsilon \qquad (16)$$

$$x_{CO_2} = x_0(1 - \exp(-\Theta/\varepsilon) - \tau_1(1 - \exp(-\Theta/\tau_1))/\varepsilon), \qquad (17)$$

where x_0 is the inlet mole fraction of CO and τ_1 is a time constant defined as $1/\tau_1 = 1/\varepsilon + Ak_1$. It should be pointed out that Eq. (17) cannot be valid at the highest temperature (638 K) because of the increased influence of the reverse reaction steps on the rate. Model (17) is fitted to the responses obtained at 563, 592, and 642 K. An example of the data fit is given in Fig. 4 where two pairs of CO_2 responses with different pretreatments are shown. The numerical values of the rate constants k_1 were obtained by estimation of τ_1 in Eq. (17) using 25 successive data points from the transient responses. The values of the constants are listed in Table 3. The constants estimated from separate experiments with different CO and H_2O partial pressures agree well with the first-order rate constants determined from stationary kinetics (Table 2).

According to the assumed mechanism (14) the constants estimated from experiments with water pretreatment should have slightly higher values than the constants obtained from the corresponding experiments without water exposure, because the number of oxygen-containing sites, O*, is in-

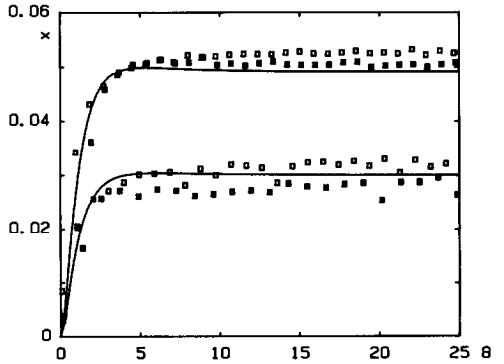

FIG. 4. Experimental and estimated (Eq. (17)) step responses of CO_2 at 592 K, experiments 7, 8, 11, and 12 (Table 3). Open symbols denote water pretreatment before reactor start-up. Θ is the dimensionless time parameter, t/τ.

TABLE 3

Rate Constants k_1 for CO_2 Formation Determined from Transient Data

Exp. No.	T (K)	$x_{H_2O,0}/x_{CO,0}$	water pretreatment[a]	$10^6 k_1$ (mol m^{-2} min^{-1} atm^{-1})
1	563	11.9	−	1.77
2	563	11.9	+	1.21
3	563	7.9	−	1.28
4	563	4.5	−	1.29
5	563	1.9	−	1.45
6	563	2.0	+	1.19
7	592	11.9	−	3.79
8	592	11.9	+	4.81
9	592	7.9	+	3.81
10	592	4.5	+	3.73
11	592	1.9	−	3.79
12	592	1.9	+	4.26

[a] +, pretreated; −, not pretreated.

creased during water treatment. The CO_2 responses, however, are quite rapid, and the differences between the responses are too small to be systematically observable in the constants given in Table 3. In most cases the initial rate of CO_2 formation was in fact slightly greater in experiments with water preadsorption. The good overall fit of the first-order rate law for CO_2 evolution suggests that the change of surface oxygen is small during the transient period; i.e., the number of oxygen containing sites (O*) is large compared to the number of vacant sites (*).

For water cleavage and hydrogen desorption processes three rival mechanisms are considered. The simplest one consists of only one reaction step:

$$H_2O + * \rightarrow H_2 + O* \qquad (18)$$

If water is assumed to adsorb on the catalyst, but the hydrogen adsorption is negligible, the conversion occurs in two steps:

$$H_2O + * \rightleftarrows H_2O* \quad \text{(fast)} \quad \text{(I)}$$
$$H_2O* \rightarrow H_2 + O* \quad \text{(slow)} \quad \text{(II)} \qquad (19)$$

This form of H_2O interconversion mechanism was used by Tinkle and Dumesic (*15*) for derivation of a steady-state rate equation.

If also H_2 is adsorbed on the surface a three-step mechanism can be written as

$$H_2O + * \rightleftarrows H_2O* \quad \text{(fast)} \quad \text{(I)}$$
$$H_2O* + O* \rightleftarrows 2OH* \quad \text{(fast)} \quad \text{(II)}$$
$$2OH* \rightarrow H_2 + 2O* \quad \text{(slow)} \quad \text{(III)} \qquad (20)$$

Each of Eqs. (18), (19), and (20) can be combined with Eq. (14) to give a complete mechanism for the shift reaction. The effect of the reversible reaction is neglected in the slow steps, since the model will be applied only to the data obtained at the lowest temperatures.

Mechanism (18) gives the rate of hydrogen evolution,

$$r_{H_2} = k_2 x_{H_2O} PL(1 - \theta_O), \qquad (21)$$

where $1 - \theta_O = \theta_v$ gives the fraction of oxygen free surface sites and L is the surface sorption capacity (in mol/m^2).

Mechanism (19) gives a rate expression with a weaker dependence on water pressure than mechanism (18), because water is assumed to be strongly adsorbed on the surface. The fraction of water on the surface is calculated from the fast step (I) in (19). The fraction of vacant sites can be expressed with the fraction of oxygen sites using the site balance:

$$\theta_v = (1 - \theta_O)/(1 + K_{H_2O} P x_{H_2O}). \qquad (22)$$

The hydrogen formation rate is determined by step (II) in Eq. (19):

$$r_{H_2} = k_2 L \theta_{H_2O} = k_2 L K_{H_2O} P x_{H_2O}(1 - \theta_O)/(1 + K_{H_2O} P x_{H_2O}). \qquad (23)$$

If the partial pressure of water is high, Eq. (23) can be approximated by

$$r_{H_2} = k_2 L(1 - \theta_O) \qquad (24)$$

which implies that the reaction rate is independent of the H_2O partial pressure.

Mechanism (20) gives a more complicated rate equation due to the nonlinear desorption step (III) involved. After applying

the quasiequilibrium approximation to the adsorption (I) and decomposition (II) steps the fractions of surface water and hydrogen are obtained: $\theta_{H_2O} = K_{H_2O}Px_{H_2O}\theta_v$ and $\theta_{OH}^2 = K_{OH}K_{H_2O}Px_{H_2O}\theta_v\theta_O$. The use of the site balance ($\theta_O + \theta_v + \theta_{OH} + \theta_{H_2O} = 1$) gives the quadratic equation

$$K_{OH}K_{H_2O}Px_{H_2O}\theta_v\theta_O = [1 - \theta_O - (1 + K_{H_2O}Px_{H_2O})\theta_v]^2. \quad (25)$$

If the number of vacant surface sites (*) is small compared to the oxygen-containing sites (O*, OH*, and H_2O*), the second-order term $(1 + K_{H_2O}Px_{H_2O})^2\theta_v^2$ becomes negligible in (25) and the fraction of vacant sites can be calculated from

$$\theta_v = \frac{(1 - \theta_O)^2}{K_{H_2O}K_{OH}Px_{H_2O}\theta_O + 2(1 - \theta_O)(1 + K_{H_2O}Px_{H_2O})}. \quad (26)$$

The H_2 formation rate is thus given by

$$r_{H_2} = k_2L^2\theta_{OH}^2 = \frac{k_2L^2K_{OH}K_{H_2O}Px_{H_2O}\theta_O(1 - \theta_O)^2}{K_{OH}K_{H_2O}Px_{H_2O}\theta_O + 2(1 - \theta_O)(1 + K_{H_2O}Px_{H_2O})}. \quad (27)$$

If water pressure is high and the original fraction of O* is much higher than the original fraction of vacant sites, (*), the most radical simplification of (27) is justified:

$$r_{H_2} = k_2L^2(1 - \theta_O)^2. \quad (28)$$

The rival rate equations (21), (24), and (28) are tested by fitting the H_2 responses from experiments with water preadsorption. Since the inlet gas was always H_2-free the material balance for H_2 can be written as

$$dx_{H_2}/d\Theta = -x_{H_2}/\varepsilon + Ar_{H_2} \quad (29)$$

The balance for oxygen-containing sites is

$$d\theta_O/d\Theta \cdot L = \tau(r_{H_2} - r_{CO_2}). \quad (30)$$

The rate of CO_2 formation is given by Eq. (15) where $c^*_O = L\theta_O$. Rate equation (15) was approximated by $r_{CO_2} = k_1Px_{CO}$. This simplification with the analytical solution, Eq. (17), is used also in computing the surface oxygen content from Eq. (30).

Since the surface sorption capacity (L) is unknown, the variable $y = L(1 - \theta_O)$ is introduced. The surface balance (30) is converted to

$$dy/d\Theta = \tau(r_{CO_2} - r_{H_2}). \quad (31)$$

The coupled differential equations (29) and (31) must in the general case be solved numerically during the parameter estimation. Rate equation (24) is, however, an exception. Inserting Eq. (24) in Eq. (3) gives a linear differential equation with respect to y ($r_{H_2} = k_2y$). Equation (31) is solved first and the function $y = f(t)$ is then inserted in the balance of H_2, Eq. (29). An analytical solution for H_2 can thus be obtained, corresponding to the rate expression (24). With the initial condition $y(0) = 0$ the solution for x_{H_2} becomes

$$x_{H_2} = x_0(1 - \tau_1/\varepsilon)(1 - \exp(-\Theta/\varepsilon)) + \frac{x_0\tau_2}{\varepsilon}\left(1 - \frac{\tau_1}{\varepsilon}\right)\frac{(\exp(-\Theta/\varepsilon) - \exp(-\Theta/\tau_2))}{(\tau_2/\varepsilon - 1)(1 - \tau_1/\tau_2)} + \frac{x_0\tau_1}{\varepsilon}\frac{(\exp(-\Theta/\varepsilon) - \exp(-\Theta/\tau_1))}{(\tau_2/\tau_1 - 1)}, \quad (32)$$

where x_0 is the inlet mole fraction of CO and τ_1 and τ_2 denote time constants defined as $1/\tau_1 = 1/\varepsilon + Ak_1$ and $1/\tau_2 = k_2\tau$.

The program package Reproche (*23, 24*) was used in most estimations. The optimization problem was solved by a Marquardt algorithm and the numerical solution of the differential equations arising from the use of rate models (21) and (28) was performed with a semi-implicit Runge–Kutta method (*24*). Simulations of the step responses with the estimated rate constants were performed with a catalytic reactor simulation package developed at our laboratory (*25*).

The H_2 responses obtained at 563 and 592 K were used in parameter estimation. Model (21) gave a reasonable fit to H_2 responses; the inflection point, however, was predicted to occur earlier than observed experimentally. The major deficiency of model (21) appeared in consideration of the estimated rate constants: the numerical value of k_2 was dependent on the water partial pressure, the product $k_2x_{H_2O}$ being ap-

TABLE 4

Rate Constants k_2 for H_2 Formation Determined from Transient Data

Exp. No.	T (K)	water pre-treatment	k_2 (min^{-1}) (Eq. (24))	$10^{-5}\,k_2$ ($m^2\,mol^{-1}\,min^{-1}$) (Eq. (28))
1	563	−	0.118	5.16
2	563	+	0.079	2.18
3	563	−	0.101	3.16
4	563	−	0.118	3.93
5	563	−	0.131	3.88
6	563	+	0.128	3.58
7	592	−	0.083	1.54
8	592	+	0.107	2.59
9	592	+	0.132	3.56
10	592	+	0.194	6.08
11	592	−	0.137	2.96
12	592	+	0.164	3.87

proximately constant. This result is consistent with the steady-state rate data: the influence of water concentration on the kinetics was minor (Fig. 1).

The parameter estimation procedure was repeated using model (24). The rate constants determined from separate experiments are given in Table 4. The numerical values were obtained from the approximate solution, Eq. (32), taking 30 successive observations at the reactor start-up. The values of k_2 are essentially concentration independent, as can be seen from Table 4. Examples of the data fitting are given in Figs. 5a and 5b, which correspond to the limiting inlet ratios of CO and H_2O at 563 K, 1 : 2 and 1 : 12, respectively. The continuous H_2 responses in Fig. 5 simulated with the estimated parameters k_1 and k_2 have a systematic deviation from the data: the inflection point of the H_2 transient was predicted erroneously, in the same way as using model (21). A typical value for the residual sum of squares was 0.2×10^{-3}. This residual is mainly caused by the inability of model (24) to fit the data, not by experimental scattering as can be seen from Fig. 5. Only two examples were shown here; the same phenomenon was observable in data fitting to all experiments, even if it was best visible at the lowest temperature, 563 K, with the slowest transients. Two different explanations can, in principle, be given: either the assumption of the rapidity of the water adsorption step is erroneous or the conversion of water is a consecutive process including adsorbed hydrogen on the catalyst surface.

The third model tested, Eq. (28), is in fact based on the assumption of slow hydrogen desorption. The model was fitted to the same data as the previous models. The estimated constants are listed in Table 4. A characteristic value for the residual sum of squares was 0.15×10^{-3}, i.e., a slightly lower value than for model (24). For the sake of comparison, the fits to the same

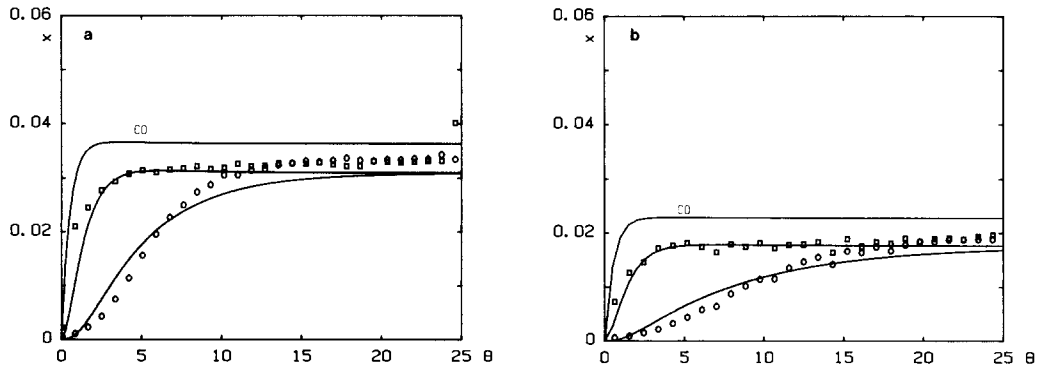

FIG. 5. Experimental and estimated step responses of H_2 (○) (Eq. (32)), CO_2 (□), and CO at 563 K at the lowest (a) and highest (b) H_2O : CO inlet ratios (experiments 6 and 2, Table 4); water pretreatment.

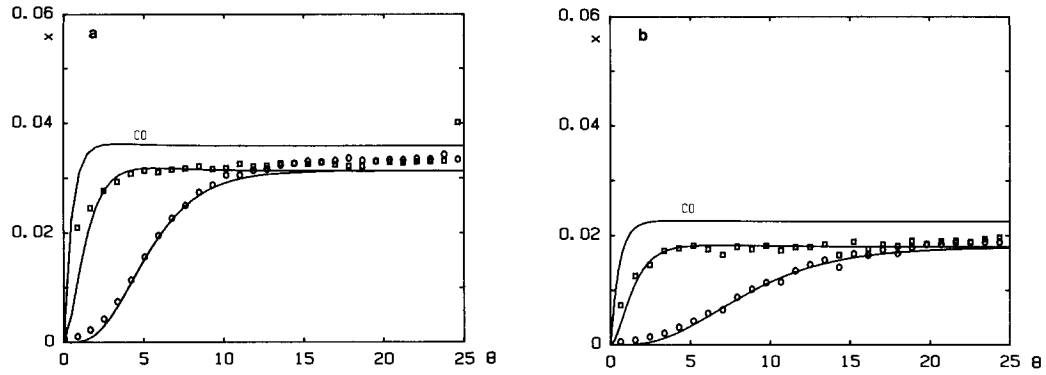

FIG. 6. Experimental and estimated step responses of H_2 (○) (Eq. (28)), CO_2 (□), and CO at 563 K at the lowest (a) and highest (b) H_2O : CO inlet ratios (experiments 6 and 2, Table 4); water pretreatment.

transient runs as those in Fig. 5 are shown in Fig. 6. It is quite evident that model (28) can better describe the overall behavior. The form of the H_2 response is predicted correctly (Fig. 6) and the residual sum of squares is caused merely by experimental scattering.

The results support the assumption that the water interconversion proceeds through fast adsorption and dissociation steps followed by a slow hydrogen desorption step. We cannot, however, exclude the possibility of the existence of more than one slow reaction step in the H_2O decomposition process. This kind of hypothesis, however, would increase the number of parameters in the model. Rate equation (28) is the simplest way to describe the hydrogen transients and it is preferable to the rival model (24) throughout the experimental domain.

At the following stage the modeling of H_2 responses was continued with experiments performed without H_2O pretreatment (responses of type b in Fig. 2) using the best model, Eq. (28). Here a new parameter appears: the initial concentration of vacant sites, which in this case cannot be approximated to be equal to zero, must be estimated in some way. Two comparative methods were used: the initial concentration was computed from the differences Δc^*_O (Fig. 3) between the identical experiments with and without water pretreatment, and, alternatively, the initial concentration was estimated simultaneously with k_2 by regression analysis. The former method gave constants which are in accordance with those determined from experiments with preadsorption, as can be seen from Table 4. The fit to the H_2 transient, however, was not very good, even though it was qualitatively correct: usually a slightly too rapid H_2 response is predicted. An example is given in Fig. 7. From the point of validity of mechanism (20) this defect should not be taken very seriously, since model equation (28) is an ultimate simplification, which is assumed to be valid after saturating the catalyst surface by water and its conversion products.

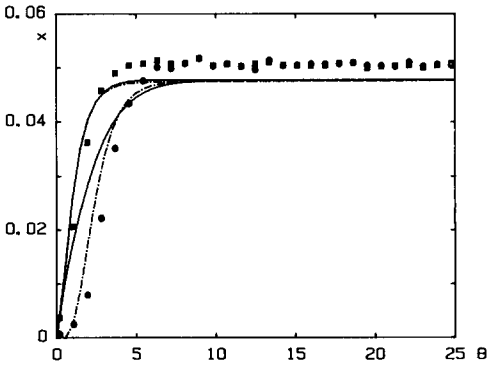

FIG. 7. Experiment 11 (Table 4) and simulated step responses (Eq. (28)) of CO_2 (■) and H_2 (●) using the rate constant k_2 in Table 4 (—) and using the rate constant determined by simultaneous estimation of k_2 and $y(0)$ (Eq. (31)) (–·–).

If the initial concentration of vacant sites and rate parameter k_2 were determined simultaneously a very good fit to the H_2 responses was achieved, the sum of residual squares being typically about 0.2×10^{-3}. An example is given in Fig. 7. The conflict, however, appears in constant k_2: values of k_2 an order of magnitude higher than those from experiments with water pretreatment were obtained (Table 4). The contradiction is, of course, due to the invalidity of the simplified model, Eq. (28), to describe the starting situation with a fresh catalyst. It should be noted, however, that model (28) can be used for prediction of H_2 transients also in this case for reactor engineering purposes.

CONCLUSIONS

The kinetic experiments performed at 563–665 K indicate that the rate of the water–gas shift reaction over a chromium-promoted magnetite catalyst is controlled by the interconversion rate of CO and desorption rate of hydrogen, whereas the adsorption of H_2O is rapid. A mechanism based on suggestions given in the recent literature (*15, 16*) was used for derivation of a simplified model for CO_2 and H_2 transients. The model predicts approximately first- and zero-order stationary kinetics with respect to CO and H_2O, respectively. The transients of CO_2 being almost independent of the catalyst pretreatment (Fig. 4) could be described by first-order kinetics (Eq. (17)). The transients of H_2 were retarded by water preadsorption (Figs. 2b and 2c) indicating the formation of stable adsorption species different from hydrogen. The H_2 responses were best modeled by an approximately second-order rate equation (Eq. (28)) with respect to vacant surface sites. The rival model, Eq. (32), based on the linear rate equation (24) was also able to predict the main characteristics of the H_2 responses. The number of oxygen-containing surface sites is large compared to vacant sites during the reaction; this is probably the reason for the almost first-order behavior of the CO_2 transients. The validity of the suggested simplified dynamic model is restricted to conditions where diffusional resistance is absent and the reversible shift process is negligible; an extension of the model would require separate adsorption measurements.

NOMENCLATURE

A	parameter, $A = \sigma\rho_c(1-\varepsilon)\tau RT/(\varepsilon P)$
$\mathbf{c}^*$	concentration vector, surface species
k, $\mathbf{k}$	rate constant, rate constant vector
K, $\mathbf{K}$	equilibrium constant, equilibrium constant vector
L	surface sorption capacity
P	total pressure (in atm)
r	reaction rate
$\mathbf{r}$, $\mathbf{r}^*$	reaction rate vectors for gas phase compounds and surface species, respectively
R	gas constant
t	time
T	temperature
x, $\mathbf{x}$	mole fraction, mole fraction vector
y	variable, defined in Eq. (31)
β	parameter, defined in Eq. (5)
ε	void fraction
θ	fractional coverage of surface species
Θ	dimensionless time, $\Theta = t/\tau$
ρ_c	skeletal density of the catalyst
σ	specific surface area of the catalyst
τ	reactor space time, τ = reactor volume/volumetric flow rate
τ_1, τ_2	time constants, defined in Eqs. (16), (17), and (32)

ACKNOWLEDGMENT

The authors express their sincere thanks to Dr. P. Valkó (Eötvös Lorand University, Budapest) for providing the computer code for regression analysis.

REFERENCES

1. Newsome, D. S., *Catal. Rev. Sci. Eng.* **21,** 275 (1980).
2. Kulkova, N. V., and Temkin, M. I., *Zh. Fiz. Khim.* **23,** 695 (1949).
3. Hulburt, H. M., and Srini Vasan, G. D., *AIChE J.* **7,** 143 (1961).
4. Moe, J. M., *Chem. Eng. Prog.* **58,** 33 (1962).

5. Shchibrya, G. G., Morozov, M. M., and Temkin, M. I., *Kinet. Katal.* **6,** 1057 (1965).
6. Glavachek, V., Marek, M., and Korzhinkova, M., *Kinet. Katal.* **9,** 1107 (1968).
7. Bohlbro, H., "An Investigation on the Kinetics of the Conversion of Carbon Monoxide with Water Vapour over Iron Oxide Based Catalysts," 2nd ed. Gjellerup, Copenhagen, 1969.
8. Fott, P., Vosolsobe, J., and Glaser, V., *Collect. Czech. Chem. Commun.* **44,** 652 (1979).
9. Chinchen, G. C., Logan, R. H., and Spencer, M. S., *Appl. Catal.* **12,** 69 (1984).
10. Boreskov, G. K., Yur'eva, T. M., and Sergeeva, A. S., *Kinet. Katal.* **11,** 1476 (1970).
11. Oki, S., Happel, J., Hnatow, M., and Kaneko, Y., "Proceedings, 5th International Congress on Catalysis, Palm Beach, 1972" (J. W. Hightower, Ed.), Vol. 1, p. 173. North-Holland/American Elsevier, Amsterdam/New York, 1973.
12. Oki, S., and Mezaki, R., *J. Phys. Chem.* **77,** 447 (1973).
13. Oki, S., and Mezaki, R., *J. Phys. Chem.* **77,** 1601 (1973).
14. Kubsh, J. E., Chen, Y., and Dumesic, J. A., *J. Catal.* **71,** 192 (1981).
15. Tinkle, M., and Dumesic, J. A., *J. Catal.* **103,** 65 (1987).
16. Salmi, T., Lindfors, L.-E., and Boström, S., *Chem. Eng. Sci.* **41,** 929 (1986).
17. Singh, C. P. P., and Saraf, D. N., *Ind. Eng. Chem. Proc. Des. Dev.* **16,** 313 (1977).
18. Mars, P., *Chem. Eng. Sci.* **14,** 375 (1961).
19. Ruthven, D. M., *Canad. J. Chem. Eng.* **47,** 327 (1969).
20. Rethwisch, D. G., Phillips, J., Chen, Y., Hayden, T. F., and Dumesic, J. A., *J. Catal.* **91,** 167 (1985).
21. Sen, S. P., Singh, S. K., Sen, B., and Chakravorty, K. R., *Indian J. Technol.* **2,** 265 (1964).
22. Kubsh, J. E., and Dumesic, J. A., *AIChE J.* **28,** 793 (1982).
23. Vajda, S., and Valkó, P., "Reproche, Manual." European Committee for Computers in Chemical Engineering Education, 1985.
24. Valkó, P., and Vajda, S., *Comput. Chem.* **8,** 255 (1984).
25. Salmi, T., *Comp. Chem. Eng.* **11,** 83 (1987).